

Supporting Information for

Enhancing magnetic performance of pyrazine-N-oxide bridged dysprosium chains through controlled variation of ligand coordination modes

Xiao-Qin Ji,^a Jin Xiong,^c Rong Sun,^c Fang Ma,^a Hao-Ling Sun,*^a Yi-Quan Zhang,^b and Song Gao*^c

^a Department of Chemistry and Beijing Key Laboratory of Energy Conversion and Storage Materials, Beijing Normal University, Beijing 100875, P. R. China. E-mail: haolingsun@bnu.edu.cn;

^b Jiangsu Key Laboratory for NSLSCS, School of Physical Science and Technology, Nanjing Normal University, Nanjing 210023, P. R. China. E-mail: zhangyiquan@njnu.edu.cn;

^c Beijing National Laboratory for Molecular Sciences, State Key Laboratory of Rare Earth Materials Chemistry and Applications, College of Chemistry and Molecular Engineering, Peking University, Beijing 100871, China. E-mail: gaosong@pku.edu.cn;

Experimental Section

Elemental analyses of carbon, hydrogen, and nitrogen were carried out with an ElementarVario EL analyzer. FTIR spectra were recorded in the range of 4000 to 400 cm⁻¹ on an AVATAR 360 Nicolet 380 FT/IR spectrometer using KBr pellets. Powder X-ray diffraction (XRD) analyses were performed on a Rigaku Dmax-2000 X-ray diffractometer with Cu K α ($\lambda=1.54059$ Å) radiation. Variable-temperature magnetic susceptibility measurements of **1** and **2** were performed on Quantum Design PPMS magnetometer (100~10000 Hz) and Quantum Design SQUID-MPMS3 (1~1000 Hz) magnetometer.

Computational details

For complexes **1** and **2**, there are two or one types of Dy³⁺ fragments, and thus we extracted two or one Dy³⁺ fragments (see Fig. 14 for the model structure of the calculated Dy³⁺ fragment) from **1** and **2** on the basis of single-crystal X-ray determined geometry. Complete-active-space self-consistent field (CASSCF) calculations on individual Dy³⁺ fragment have been carried out with MOLCAS 8.2 program package.^{S1} The basis sets for all atoms are atomic natural orbitals from the MOLCAS ANO-RCC library: ANO-RCC-VTZP for Dy³⁺ ion; VTZ for close O and N; VDZ for distant atoms. During the calculation, the close Dy³⁺ ion was replaced by diamagnetic Lu³⁺. The calculations employed the second order Douglas-Kroll-Hess Hamiltonian, where scalar relativistic contractions were taken into account in the basis set and the spin-orbit couplings were handled separately in the restricted active space state interaction (RASSI-SO) procedure. For the fragment of individual Dy³⁺ ion, active electrons in 7 active spaces include all *f* electrons (CAS (9 in 7)) in the CASSCF calculation. To exclude all the doubts, we calculated all the roots in the active space. We have mixed the maximum number of spin-free state which was possible with our hardware (all from 21 sextets, 128 from 224 quadruplets, 130 from 490 doublets).

Fitting the exchange interaction in two complexes using Lines model based on CASSCF results

To fit the exchange interactions in complexes **1** and **2**, we took two steps to obtain them. Firstly, we calculated the mononuclear fragment using CASSCF to obtain the corresponding magnetic properties (see the first part). And then, the exchange interaction between the magnetic centers is considered within the Lines model,^{S2} while the account of the dipole-dipole magnetic coupling is treated exactly. The Lines model is effective and has been successfully used widely in the research field of binuclear lanthanide single-molecule magnets.^{S3}

For complexes **1** and **2**, we only consider one type of Dy³⁺-Dy³⁺ interactions. The exchange Hamiltonian can be expressed as follow: $\hat{H}_{exch} = -J_{total} \hat{\tilde{S}}_{Dy1} \hat{\tilde{S}}_{Dy1A}$.

The J_{total} is the parameter of the total magnetic interaction ($J_{total}=J_{dipolar}+J_{exchange}$)

between Dy³⁺ ions. The $\hat{S}_{Dy} = \pm 1/2$ is the ground pseudospin on the Dy³⁺ site. The dipolar magnetic coupling can be calculated exactly, while the exchange coupling constant was fitted through comparison of the computed and measured magnetic susceptibility using the POLY_ANISO program.^{S4}

Table S1. Selected Bond Distances (\AA) in complexes **1** and **2**

1-Dy1		1-Dy2		2	
Dy1-O1	2.162(4)	Dy2-O4	2.172(4)	Dy1-O1	2.164(7)
Dy1-O2	2.351(3)	Dy2-O2	2.384(4)	Dy1-O2	2.356(7)
Dy1-O5	2.389(4)	Dy2-O5	2.339(3)	Dy1-O2#1	2.354(7)
Dy1-O6	2.361(4)	Dy2-O7	2.446(4)	Dy1-O3#2	2.401(7)
Dy1-O9#1	2.462(4)	Dy2-O8	2.389(4)	Dy1-O4	2.353(7)
Dy1-N1	2.507(5)	Dy2-N5	2.438(5)	Dy1-N1	2.501(8)
Dy1-N3	2.579(5)	Dy2-N8	2.559(5)	Dy1-N4#1	2.602(8)
Dy1-Cl1	2.744 (16)	Dy2-Cl2	2.729(17)	Dy1-Cl1	2.726(2)

Symmetry code for **1**: #1: 1-x, -1/2+y, 1/2-z

Symmetry code for **2**: #1: 1-x, 2-y, 1-z

Table S2. Hydrogen Bonds in **1**.

D-H	d(D-H) (\AA)	\angle DHA ($^{\circ}$)	d(D...A) (\AA)	A
C6-H6a	0.9300	153.72	3.706	Cl2 [3-x, 1-y, 1-z]
C7-H7a	0.9301	161.05	3.624	Cl2 [3-x, 1-y, 1-z]
C10-H10	0.9300	137.73	3.661	Br1 [4-x, 1-y, 1-z]
C18-H18	0.9301	161.05	3.624	Cl1 [1-x, -y, 1-z]
C18-H18	0.9301	149.38	3.713	Cl2 [x, 0.5-y, 0.5+z]
C24-H24	0.9299	137.87	3.123	O3 [x, 0.5-y, 0.5+z]

Table S3. Hydrogen Bonds in **2**.

D-H	d(D-H) (\AA)	\angle DHA ($^{\circ}$)	d(D...A) (\AA)	A
C13-H13	0.930	171.00	3.670	Cl1 [-x, 2-y, 1-z]
C12-H12	0.930	130.09	3.503	Cl1 [-x, 2-y, 1-z]
C3-H3	0.930	146.44	3.838	Br1 [1+x, -2+y, 1+z]

Table S4. Relaxation fitting parameters from Least-Squares Fitting of $\chi(f)$ data under zero dc field of 1.

T (K)	χ_t	χ_s	α	τ (s)
5	7.49	0.090	0.26	0.60
5.5	6.32	0.086	0.25	0.35
6	5.56	0.082	0.24	0.21
6.5	4.89	0.079	0.24	0.13
7	4.40	0.078	0.23	0.088
7.5	4.02	0.075	0.22	0.061
8	3.70	0.074	0.22	0.043
8.5	3.44	0.072	0.21	0.031
9	3.23	0.072	0.21	0.023
9.5	3.04	0.071	0.21	0.018
10	2.87	0.070	0.21	0.014
10.5	2.72	0.072	0.20	0.011
11	2.59	0.071	0.20	0.0083
11.5	2.46	0.071	0.20	0.0066
12	2.36	0.068	0.20	0.0053
12.5	2.25	0.069	0.20	0.0042
13	2.15	0.069	0.19	0.0034
13.5	2.07	0.071	0.19	0.0028
14	1.99	0.067	0.19	0.0022
14.5	1.91	0.070	0.19	0.0018
15	1.84	0.064	0.19	0.0015
15.5	1.78	0.061	0.20	0.0012
16	1.72	0.055	0.20	9.57E-4
16.5	1.66	0.057	0.21	7.79E-4
17	1.61	0.057	0.21	6.33E-4
17.5	1.56	0.060	0.21	5.23E-4
18	1.52	0.048	0.22	4.25E-4
18.5	1.47	0.067	0.22	3.57E-4
19	1.40	0.11	0.19	3.06E-4
19.5	1.39	0.087	0.23	2.60E-4
20	1.30	0.12	0.17	2.08E-4
20.5	1.28	0.12	0.16	1.79E-4
21	1.24	0.10	0.20	1.44E-4
21.5	1.19	0.11	0.18	1.21E-4
22	1.14	0.11	0.18	1.00E-4
22.5	1.11	0.12	0.17	8.36E-5
23	1.08	0.13	0.16	7.00E-5
23.5	1.05	0.13	0.16	5.90E-5
24	1.03	0.15	0.15	5.04E-5

24.5	1.00	0.15	0.15	4.21E-5
25	0.98	0.18	0.13	3.72E-5
25.5	0.96	0.19	0.13	3.16E-5
26	0.93	0.20	0.12	2.73E-5
26.5	0.92	0.20	0.12	2.30E-5
27	0.89	0.23	0.097	2.06E-5
27.5	0.88	0.22	0.11	1.67E-5
28	0.85	0.28	0.063	1.62E-5

Table S5. Relaxation fitting parameters from Least-Squares Fitting of $\chi(f)$ data under zero dc field of 2.

T (K)	χ_t	χ_s	α	$\tau(s)$
9.5	1.97	0.028	0.14	0.28
10	1.75	0.028	0.13	0.19
10.5	1.62	0.028	0.12	0.13
11	1.49	0.029	0.11	0.097
11.5	1.34	0.035	0.077	0.070
12	1.31	0.030	0.10	0.056
12.5	1.24	0.030	0.093	0.043
13	1.18	0.033	0.079	0.034
13.5	1.13	0.031	0.086	0.027
14	1.078	0.032	0.077	0.021
14.5	1.035	0.033	0.073	0.017
15	1.00	0.033	0.072	0.014
15.5	0.96	0.035	0.064	0.011
16	0.92	0.034	0.067	0.0088
16.5	0.89	0.035	0.058	0.0071
17	0.86	0.034	0.066	0.0057
17.5	0.84	0.033	0.066	0.0046
18	0.81	0.034	0.063	0.0037
18.5	0.79	0.033	0.066	0.0030
19	0.77	0.033	0.071	0.0024
19.5	0.74	0.035	0.063	0.0019
20	0.73	0.033	0.075	0.0015
20.5	0.71	0.033	0.074	0.0012
21	0.69	0.034	0.078	9.71E-4
21.5	0.67	0.036	0.078	7.71E-4
22	0.66	0.034	0.087	6.071E-4
22.5	0.64	0.040	0.086	4.83E-4
23	0.63	0.02	0.11	3.67E-4
23.5	0.61	0.018	0.12	2.82E-4
24	0.60	0.016	0.13	2.16E-4
24.5	0.59	0.016	0.12	1.69E-4
25	0.59	0.012	0.15	1.27E-4
25.5	0.56	0.0064	0.16	1.00E-4
26	0.56	1E-5	0.18	7.55E-5
26.5	0.54	1E-5	0.18	5.73E-5
27	0.53	1E-5	0.18	4.37E-5
27.5	0.52	1E-5	0.19	3.37E-5
28	0.51	1E-5	0.19	2.61E-5
28.5	0.50	1E-5	0.20	2.04E-5

Table S6. Calculated energy levels (K), \mathbf{g} (g_x , g_y , g_z) tensors and m_J values of the lowest Kramers doublets (KDs) of the individual Dy fragments of complexes **1-2**.

KDs	1-Dy1		1-Dy2		2	
	E / K	g	E / K	g	E / K	g
1	0.0	0.002	0.0	0.005	0.0	0.001
		0.004		0.007		0.002
		19.644		19.691		19.638
2	280.0	0.072	252.7	0.064	210.7	0.006
		0.090		0.083		0.011
		16.856		16.826		17.445
3	485.7	0.461	465.4	1.850	398.8	0.148
		0.948		2.620		1.574
		17.533		12.998		16.214
4	542.4	1.806	537.6	0.398	421.1	1.355
		4.545		3.512		3.487
		10.857		14.940		12.477
6	614.9	0.134	618.7	4.277	489.4	2.705
		4.843		5.344		5.137
		11.608		9.685		10.426
7	697.4	3.751	721.6	1.325	569.0	3.075
		6.095		1.863		3.795
		9.794		13.751		9.288
8	759.4	0.350	825.5	0.244	627.7	0.395
		0.395		0.700		1.256
		15.409		17.312		13.513
9	832.9	0.158	901.3	0.085	688.4	0.672
		0.374		0.221		0.928
		18.735		19.489		18.030

Table S7. The calculated dipole-dipole interaction J_{dip} , fitted exchange coupling constant J_{exch} , and the total J ($J = J_{\text{dip}} + J_{\text{exch}}$) between Dy³⁺ ions in **1** and **2** (cm⁻¹).

		1	2
J	J_{dip}	4.19	4.35
	J_{exch}	-1.25	1.75
	J	2.94	6.10

Table S8. Some similar examples of lanthanide-based molecular nanomagnets based on $\{\text{Dy}_2\}$ subunits.

				J / cm^{-1}			Ref
	Crystal structure	Dy-Dy/ Å	Dy-O-Dy	J_{dip}	J_{exch}	J	
$[\text{Dy}_2\text{L}_2\text{Cl}_2(\text{CH}_3\text{OH})_3]_n \cdot n\text{C}_\text{H}_3\text{OH}$	1D	3.982	114.2°/ 114.8°	4.19	-1.25	2.94	This work
$[\text{Dy(L)}\text{Cl}(\text{DMF})]_n$	1D	3.990	115.9°	4.35	1.75	6.10	This work
$\{[\text{Dy}_2\text{L}_2(\text{bpdo})_2(\text{H}_2\text{O})(\text{CH}_3\text{OH})] \cdot 2\text{ClO}_4 \cdot 2\text{CH}_3\text{CN}\}_n$	3D	3.943	113.8°/ 115.0°	4.52	-0.75	3.77	12a
$\{[\text{DyL}(\text{bpdo})(\text{H}_2\text{O})] \cdot \text{ClO}_4 \cdot 2\text{H}_2\text{O}\}_n$	2D	3.973	114.8°	4.37	-1.5	2.87	12a
$[\text{DyLCl}(\text{CH}_3\text{OH})]_2$	dinuclear	3.900	113.7°	4.82	-1.00	3.82	12c
$[\text{DyL}(\text{HCOO})(\text{CH}_3\text{OH})]_n$	1D	3.938	113.4°	4.56	1.75	6.31	12c
$[\text{Dy}_2(\text{HL})_2(\text{NO}_3)_2(\text{CH}_3\text{CN})_2] \cdot 2\text{CH}_3\text{CN}$	dinuclear	3.919	114.1°	5.22	-0.75	4.47	18a
$[\text{Dy}_2(\text{HL})_2(\text{NO}_3)_2(\text{DMF})_2] \cdot 2\text{H}_2\text{O}$	dinuclear	3.942	114.5°	5.01	-0.03	4.98	18a
$\text{Dy}_2(\text{HL})_2(\text{NO}_3)_2(\text{DMF})_4$	dinuclear	4.015	114.7°	4.69	5.00	9.69	18a
$[\text{Dy}_2(\text{L})_2(\text{DBM})_2(\text{DMA})_2] \cdot 2\text{DMA} \cdot 2\text{CH}_3\text{CN}$	dinuclear	3.755	105.5°	6.03	-7.33	-1.30	18b
$[\text{Dy}_2(\text{L})_2(\text{DBM})_2(\text{DMF})_2]$	dinuclear	3.790	106.9°	5.86	-3.40	2.46	18b
$[\text{Dy}_2(\text{tfo})_4(\text{L}^2)_2(\text{EtOH})_2]$	dinuclear	3.778	107.9°	4.46	-3.25	1.21	18c

Abbreviations: $\text{H}_2\text{L} = \text{N}'\text{-}(5\text{-bromo-2-hydroxybenzylidene})\text{pyrazine-N-oxide-carbohydrazide}$; $\text{H}_2\text{L}=\text{N}'\text{-}(2\text{-hydroxybenzylidene})\text{picolinohydrazide}$; $\text{H}_3\text{L} = 3\text{-hydroxy-N}'\text{-}(2\text{-hydroxy-3-methoxybenzylidene)picolinohydrazide}$; $\text{H}_2\text{L} = 2\text{-}(2\text{-hydroxy-3-methoxybenzylideneamino)phenol}$, HDBM = dibenzoylmethane, DMA = dimethylacetamide; $\text{HL}^2 = 8\text{-hydroxyquinoline-2-carboxaldehyde-(benzoyl)hydrazine}$;

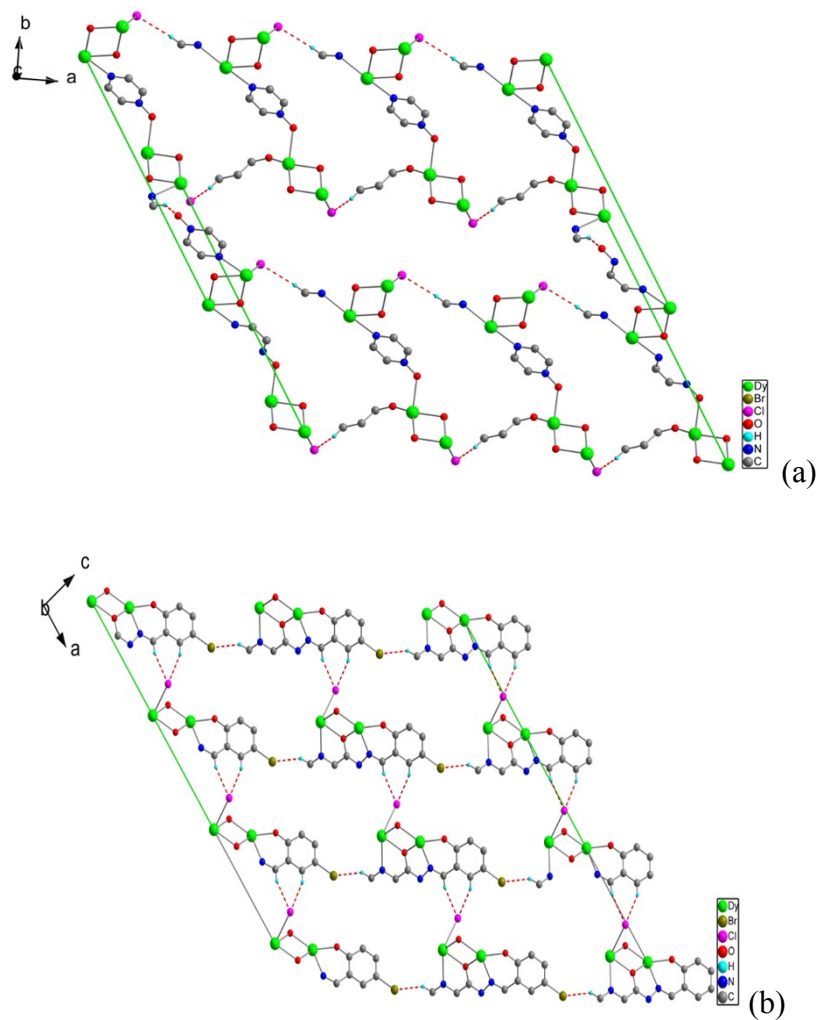


Fig. S1 The hydrogen-bonded 2D layer (a) and the connection of the hydrogen bonds between the layers (b) in **1**.

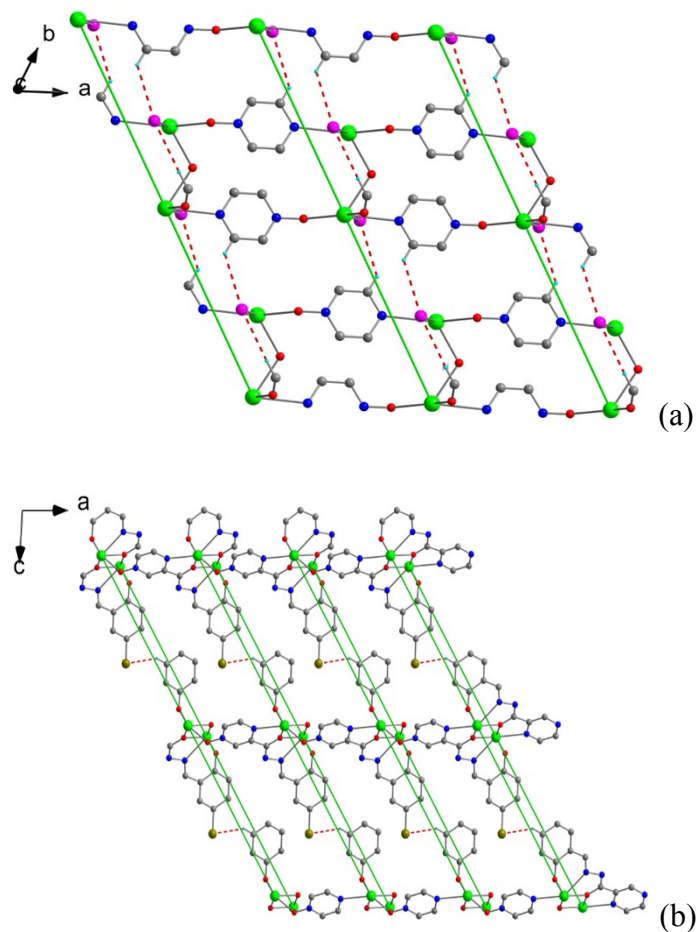


Fig. S2 The hydrogen-bonded 2D layer (a) and the connection of the hydrogen bonds between the layers (b) in **2**.

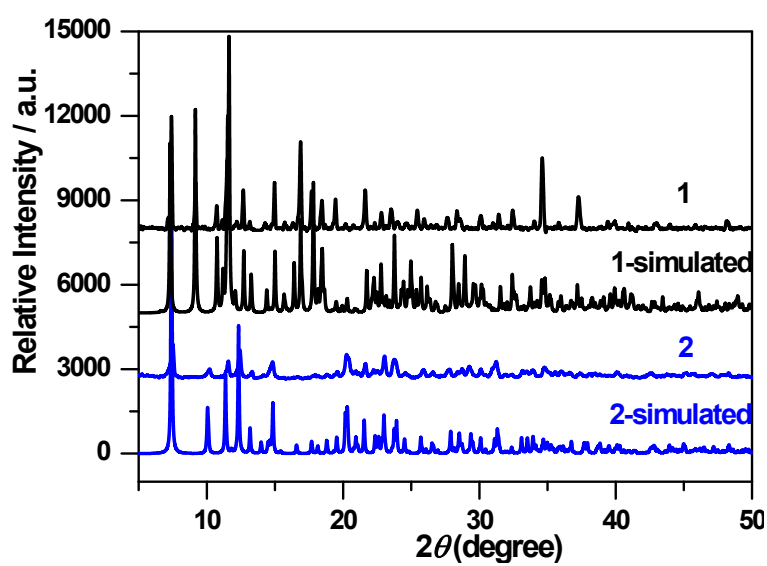


Fig. S3 Powder X-ray diffraction profiles of **1** and **2** together with a simulation from the single crystal data.

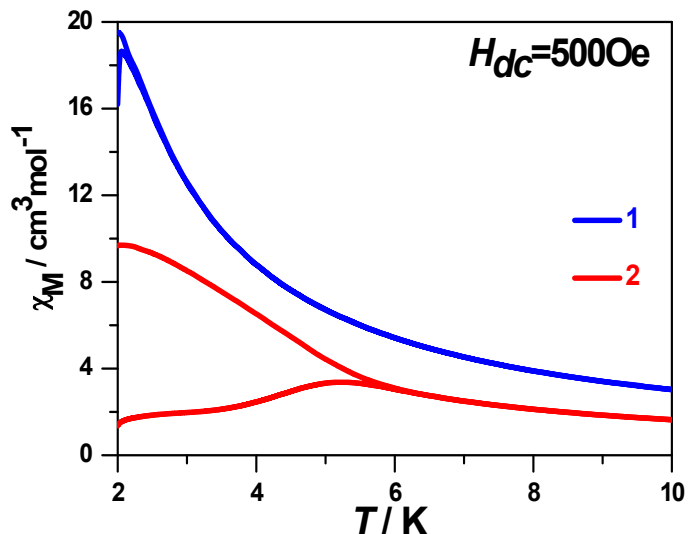


Fig. S4 The zero-field-cooled/field-cooled (ZFC-FC) magnetic susceptibilities under 500 Oe dc field with a sweep rate of 3 K/min were measured for **1** and **2**.

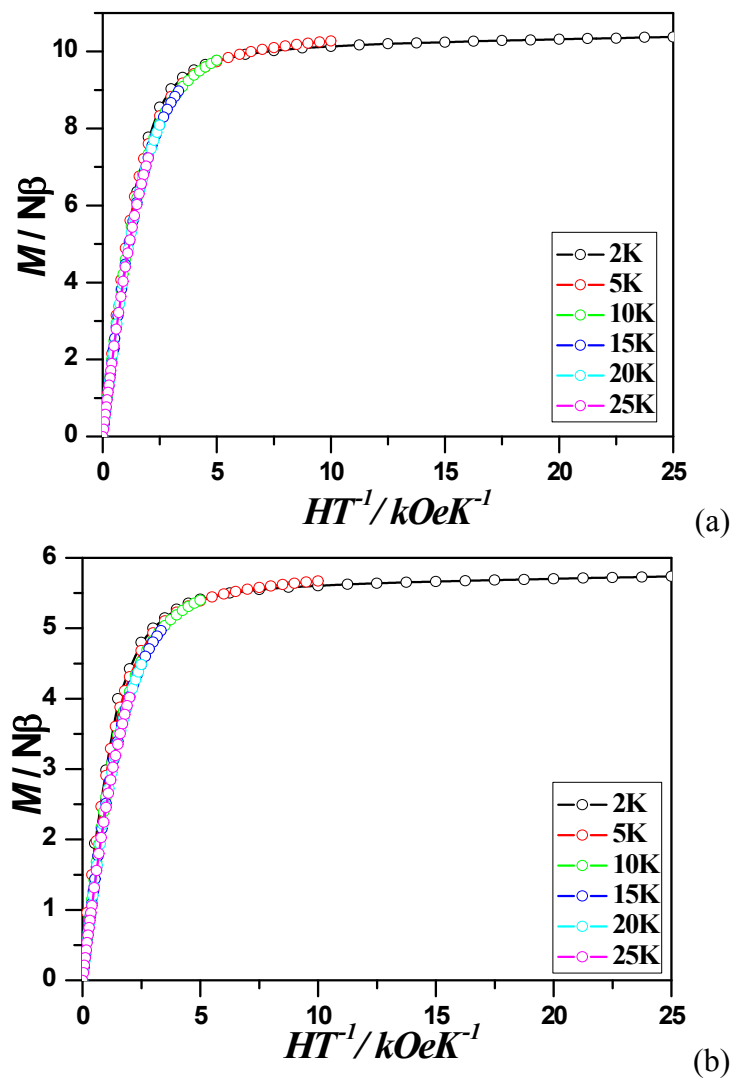


Fig. S5 Plots of M-H for **1** and **2** at 2, 5, 10, 15, 20, and 25 K, respectively

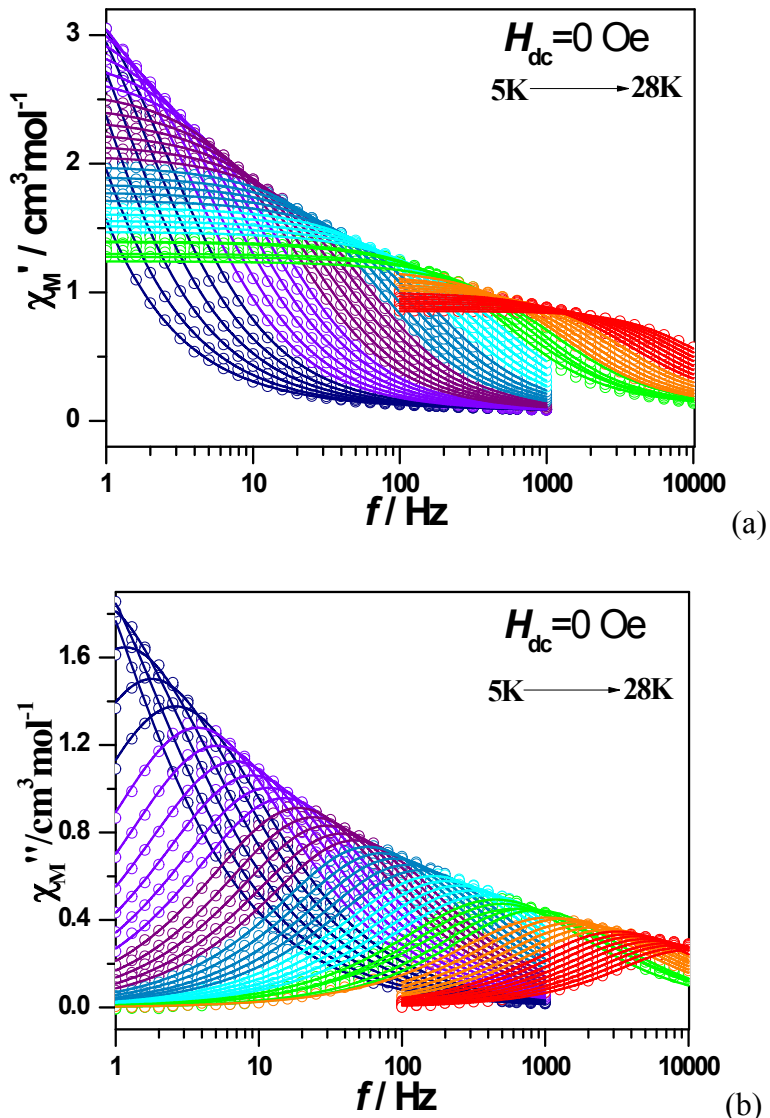


Fig. S6 $Ac-f$ curves measured under 0 kOe dc fields for **1**. Solid lines were fitted using a generalized Debye relaxation model, simultaneously to $\chi'(f)$ and $\chi''(f)$ curves.

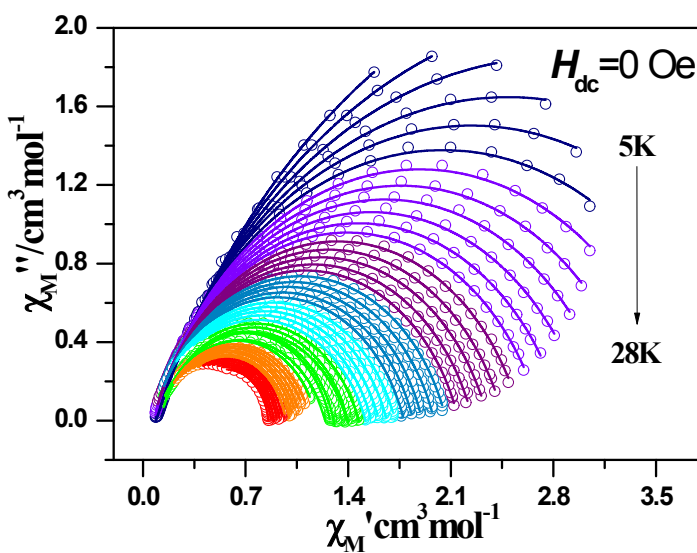


Fig. S7 Cole-Cole plots of **1** under 0 kOe dc field.

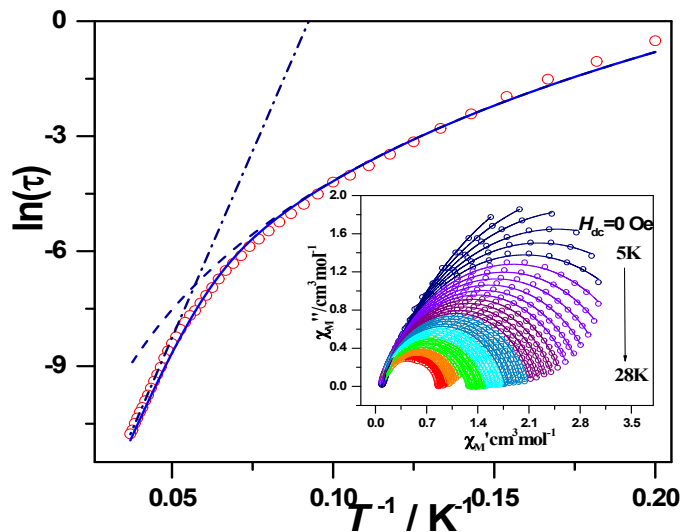


Fig. S8 Plot of $\ln(\tau)$ versus T^{-1} for **1** under zero dc field. The blue line represents the fit results with the consideration of Orbach process and Roman processes. Inset: Cole–Cole plots measured at 5.0–28 K under zero dc field, with the best fit to the generalized Debye model.

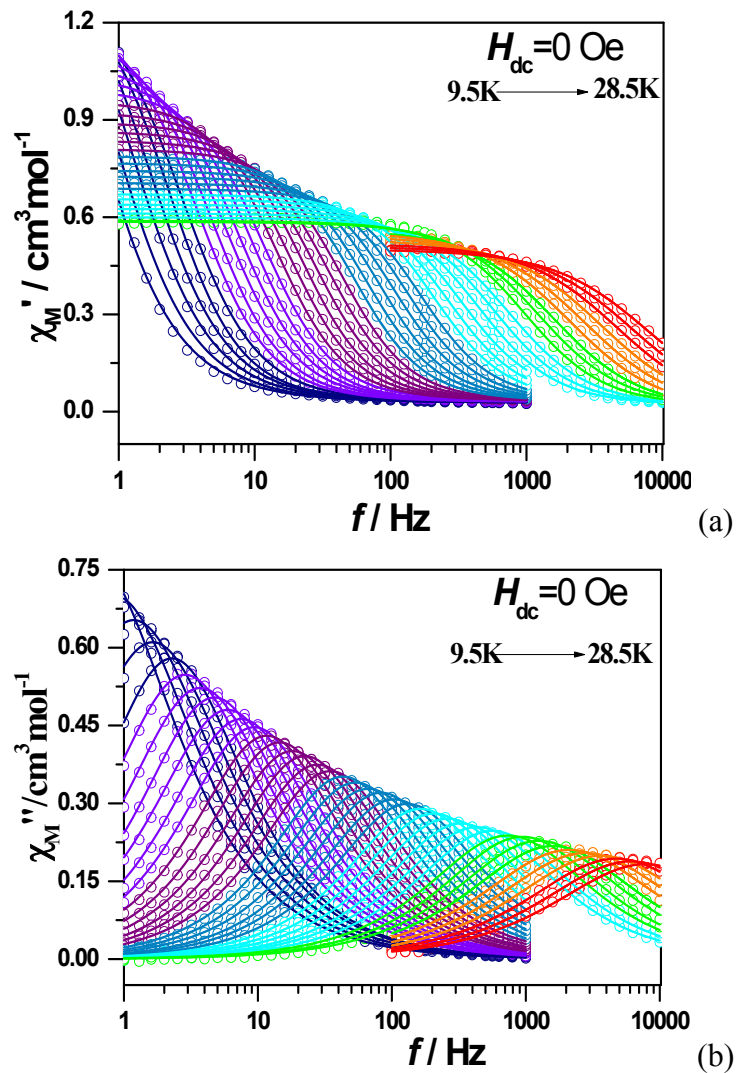


Fig. S9 $Ac-f$ curves measured under 0 kOe dc fields for **2**. Solid lines were fitted using a generalized Debye relaxation model, simultaneously to $\chi'(f)$ and $\chi''(f)$ curves.

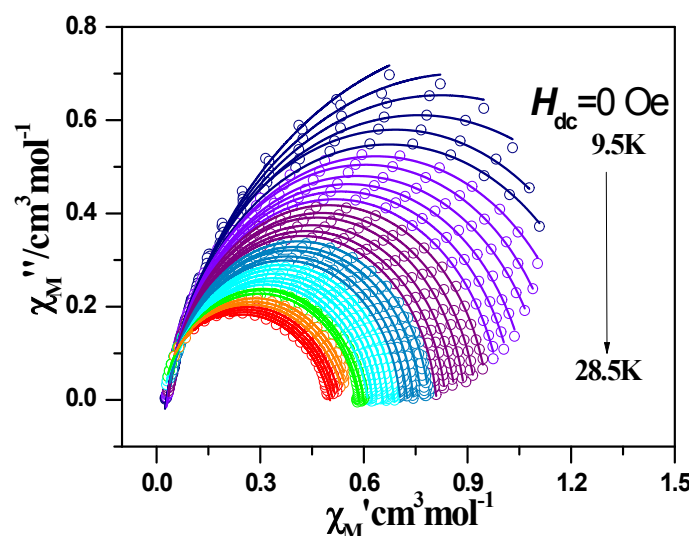


Fig. S10 Cole-Cole plots of **2** under 0 kOe dc field.

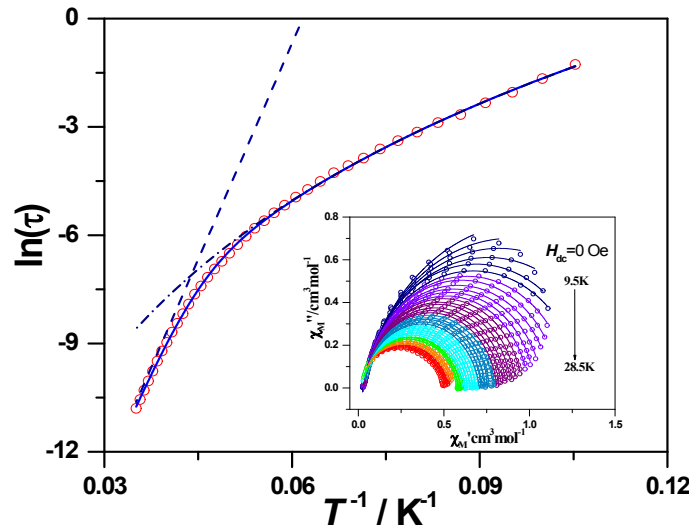
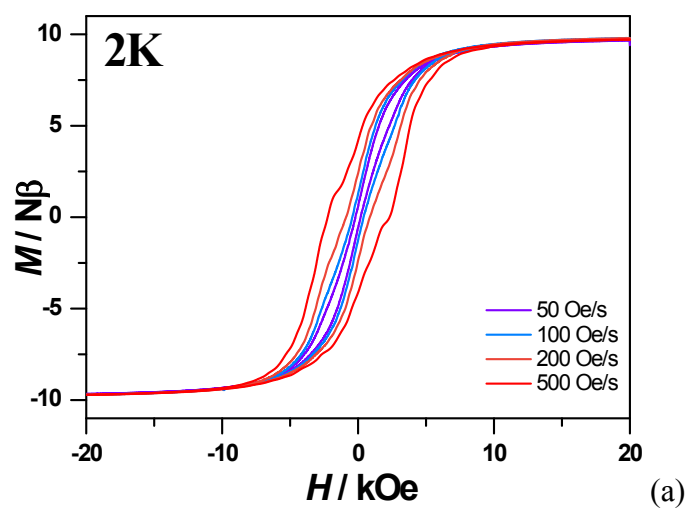
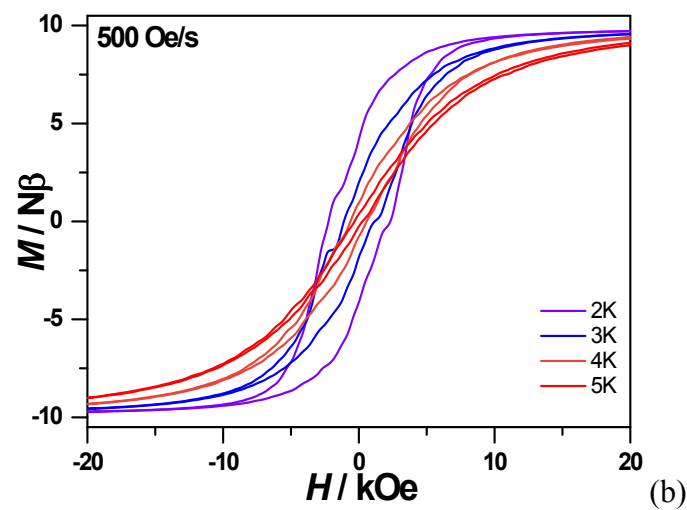


Fig. S11 Plot of $\ln(\tau)$ versus T^{-1} for **2** under zero dc field. The blue line represents the fit results with the consideration of Orbach process and Roman processes. Inset: Cole–Cole plots measured at 9.5–28.5 K under zero dc field, with the best fit to the generalized Debye model.



(a)



(b)

Fig. S12 Hysteresis loop for **1** measured with different sweep rates at 2 K (a) and different temperatures with sweep rates of 500 Oe/s (b).

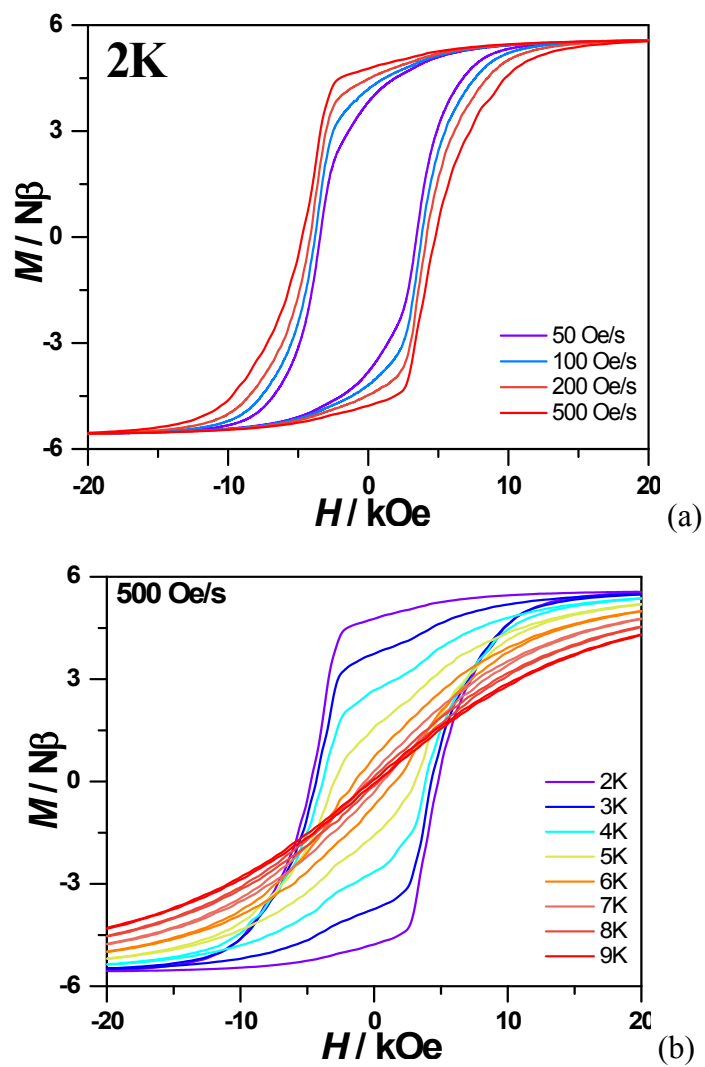


Fig. S13 Hysteresis loop for **2** measured with different sweep rates at 2 K (a) and different temperatures with sweep rates of 500 Oe/s (b).

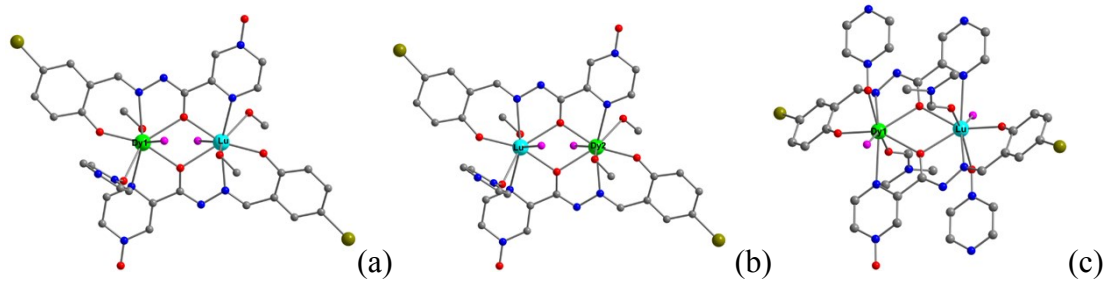


Fig. S14 Calculated model structure for complex complexes **1** (a-b) and **2** (c); H atoms are omitted.

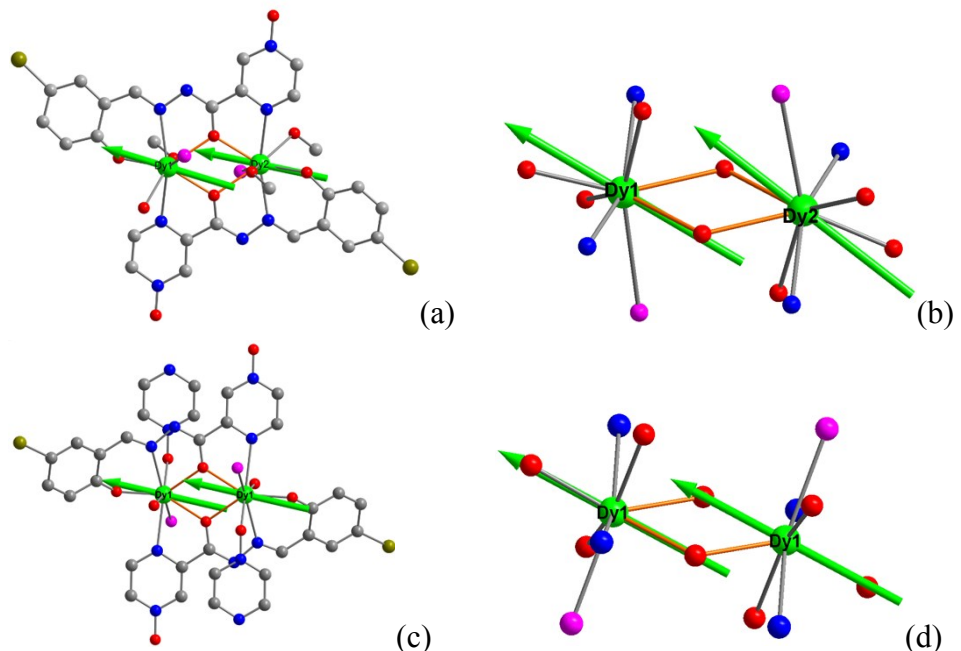


Fig. S15 Orientation of the local main magnetic axes of the ground Kramers doublet on Dy^{3+} ion of complexes **1** (a-b) and **2** (c-d).

Reference

- (1) G. Karlström, R. Lindh, P.-Å. Malmqvist, B. O. Roos, U. Ryde, V. Veryazov, P.-O. Widmark, M. Cossi, B. Schimmelpfennig, P. Neogrady and L. Seijo, *Comput. Mater. Sci.*, 2003, **28**, 222.
- (2) M. E. Lines, *J. Chem. Phys.* 1971, **55**, 2977.
- (3) (a) K. C. Mondal, A. Sundt, Y. Lan, G. E. Kostakis, O. Waldmann, L. Ungur, L. F. Chibotaru, C. E. Anson and A. K. Powell, *Angew. Chem., Int. Ed.*, 2012, **51**, 7550; (b) S. K. Langley, D. P. Wielechowski, V. Vieru, N. F. Chilton, B. Moubaraki, B. F. Abrahams, L. F. Chibotaru and K. S. Murray, *Angew. Chem., Int. Ed.*, 2013, **52**, 12014.

- (4) (a) L. F. Chibotaru, L. Ungur and A. Soncini, *Angew. Chem., Int. Ed.*, 2008, **47**, 4126; (b) L. Ungur, W. Van den Heuvel and L. F. Chibotaru, *New. J. Chem.*, 2009, **33**, 1224; (c) L. F. Chibotaru, L. Ungur, C. Aronica, H. Elmoll, G. Pilet and D. Luneau, *J. Am. Chem. Soc.*, 2008, **130**, 12445.